*Inorg. Chem.* **2005**, *44*, 6339–6345

# Comparative Electronic Band Structure Study of the Intrachain Ferromagnetic versus Antiferromagnetic Coupling in the Magnetic Oxides $Ca_3Co_2O_6$ and $Ca_3FeRhO_6$

**Antoine Villesuzanne*,† and Myung-Hwan Whangbo***

*Department of Chemistry, North Carolina State University, Raleigh, North Carolina 27695-8204*

Received June 1, 2005

In the $(MM'O_6)_\infty$ chains of the transition-metal magnetic oxides $Ca_3MM'O_6$ the $MO_6$ trigonal prisms alternate with the $M'O_6$ octahedra by sharing their triangular faces. In the $(Co_2O_6)_\infty$ chains of $Ca_3Co_2O_6$ (M = M′ = Co) the spins are coupled ferromagnetically, but in the $(FeRhO_6)_\infty$ chains of $Ca_3FeRhO_6$ (M = Fe, M′ = Rh) they are coupled antiferromagnetically. The origin of this difference was probed by carrying out spin-polarized density functional theory electronic band structure calculations for ordered spin states of $Ca_3Co_2O_6$ and $Ca_3FeRhO_6$. The spin state of a $(MM'O_6)_\infty$ chain determines the occurrence of direct metal–metal bonding between the adjacent trigonal prism and octahedral site transition-metal atoms. The extent of direct metal–metal bonding in the $(Co_2O_6)_\infty$ chains of $Ca_3Co_2O_6$ is stronger in the intrachain ferromagnetic state than in the intrachain antiferromagnetic state, so that the intrachain ferromagnetic state becomes more stable than the intrachain antiferromagnetic state. Such a metal–metal-bonding-induced ferromagnetism is expected to occur in magnetic insulators and magnetic metals of transition-metal elements in which direct metal–metal bonding can be enhanced by ferromagnetic ordering. In the $(FeRhO_6)_\infty$ chains of $Ca_3FeRhO_6$ the ferromagnetic coupling does not lead to a strong metal–metal bonding and the adjacent spins interact by the Fe–O···O–Fe super-superexchange, hence leading to an antiferromagnetic coupling.

## 1. Introduction

In the transition-metal magnetic oxides $Ca_3MM'O_6$ the $(MM'O_6)_\infty$ chains are separated by $Ca^{2+}$ cations, each $(MM'O_6)_\infty$ chain has $MO_6$ trigonal prisms alternating with $M'O_6$ octahedra by sharing their triangular faces, and these one-dimensional (1D) chains are closely packed to form a hexagonal lattice (Figure 1). The magnetic susceptibility of $Ca_3Co_2O_6$ (M = M′ = Co) is highly anisotropic and described by an Ising Hamiltonian.[1−3] To a first approximation each trigonal prism (TP) site has a high-spin $Co^{3+}$ ($d^6$ $S = 2$) ion and each octahedral (OCT) site a low-spin $Co^{3+}$ ($d^6$, $S = 0$) ion,[3−5] so that the highly anisotropic magnetic properties of $Ca_3Co_2O_6$ originate from the TP-site $Co^{3+}$ ($d^6$, $S = 2$) ions. Indeed, a recent study of crystal field and spin−orbit coupling effects showed that a high-spin $d^6$ ion at a TP site has uniaxial magnetic properties.[6] In $Ca_3Co_2O_6$ the adjacent TP-site $Co^{3+}$ ions have a strong ferromagnetic (FM) coupling in each $(Co_2O_6)_\infty$ chain while the interchain coupling is weakly antiferromagnetic (AFM).[2,3,7−10] Thus, the magnetic properties of $Ca_3Co_2O_6$ can be described in terms of a planar Ising hexagonal lattice in which the magnetic moment of each $(Co_2O_6)_\infty$ chain plays the role of one spin.[2] $Ca_3FeRhO_6$ has one less valence electron per formula unit (FU) than $Ca_3Co_2O_6$. In the $(FeRhO_6)_\infty$ chains of $Ca_3FeRhO_6$ the Fe and Rh atoms are located at the TP and OCT sites, respectively.[11−13] The $^{57}$Fe Mössbauer study of $Ca_3FeRhO_6$

* To whom correspondence should be addressed. E-mail: ville@icmcb-bordeaux.cnrs.fr (A.V.); mike_whangbo@ncsu.edu (M.-H.W.).

† Permanent address: ICMCB−CNRS, 87 Avenue du Dr. Schweitzer, 33608 Pessac Cedex France.

(1) Kageyama, H.; Yoshimura, K.; Kosuge, K.; Azuma, M.; Takano, M.; Mitamura, H.; Goto, T. *J. Phys. Soc. Jpn.* **1997**, *66*, 3996.
(2) Maignan, A.; Michel, C.; Masset, A. C.; Martin, C.; Raveau, B. *Eur. J. Phys. B* **2000**, *15*, 657.
(3) Hardy, V.; Lambert, S.; Lees, M. R.; Paul, D. Mc K. *Phys. Rev. B* **2003**, *68*, 014424.
(4) Sampathkumaran, E. V.; Fujiwara, N.; Rayaprol, S.; Madhu, P. K.; Uwatoko, Y. *Phys. Rev. B* **2004**, *70*, 014437.
(5) Whangbo, M.-H.; Dai, D.; Koo, H.-J.; Jobic, S. *Solid State Commun.* **2003**, *125*, 413.
(6) Dai, D.; Whangbo, M.-H. *Inorg. Chem.* **2005**, *44*, 4407.
(7) Aasland, S.; Fjellvåg, H.; Hauback, B. *Solid State Commun.* **1997**, *101*, 187.
(8) Kageyama, H.; Yoshimura, K.; Kosuge, K.; Mitamura, H.; Goto, T. *J. Phys. Soc. Jpn.* **1997**, *66*, 1607.
(9) Kageyama, H.; Yoshimura, K.; Kosuge, K.; Xu, X.; Kawano, S. *J. Phys. Soc. Jpn.* **1998**, *67*, 357.
(10) Martínez, B.; Laukhin, V.; Hernando, M.; Fontcuberta, J.; Parras, M.; González-Calbet, J. M. *Phys. Rev. B* **2001**, *64*, 012417.

10.1021/ic0508775 CCC: $30.25 
Published on Web 08/04/2005

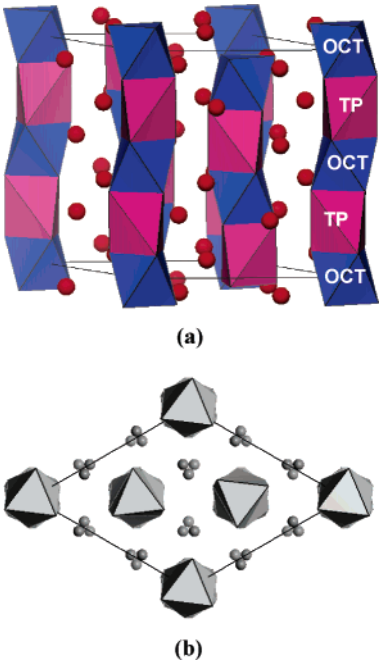


**Figure 1.** Crystal structure of $Ca_3MM'O_6$: (a) a perspective view and (b) a projection view of the $(MM'O_6)_\infty$ chains along the chain direction.

showed that each TP site has a high-spin $Fe^{3+}$ ($d^5$, $S = 5/2$) ion,[13] so it is most likely that each OCT site has a low-spin $Rh^{3+}$ ($d^6$, $S = 0$) ion. Therefore, $Ca_3FeRhO_6$ is similar to $Ca_3Co_2O_6$ in that, to a first approximation, the TP sites have unpaired spins while the OCT sites are diamagnetic. However, $Ca_3Co_2O_6$ and $Ca_3FeRhO_6$ are quite different in their magnetic properties because the spins of adjacent TP-site ions have an AFM coupling in the $(FeRhO_6)_\infty$ chains but a FM coupling in the $(Co_2O_6)_\infty$ chains. From the viewpoint of spin exchange,[14] the intrachain spin exchange between adjacent TP sites is of the super-superexchange type involving the M−O···O−M (M = Co, Fe) paths and is therefore expected to be AFM rather than FM. Thus far it is not known why $Ca_3Co_2O_6$ and $Ca_3FeRhO_6$ exhibit different intrachain spin coupling behaviors. In the present work we explore what electronic factor causes an intrachain ferromagnetism in $Ca_3Co_2O_6$ but an intrachain antiferromagnetism in $Ca_3FeRhO_6$ on the basis of density functional theory (DFT) electronic band structure calculations for $Ca_3Co_2O_6$ and $Ca_3FeRhO_6$.

## 2. Computational Details

First-principles DFT electronic band structures were calculated for nonmagnetic and magnetic states of $Ca_3Co_2O_6$ and $Ca_3FeRhO_6$ using the full-potential, all-electrons (linearized)-augmented plane wave + local orbitals (L/APW+lo) method[15,16] implemented in the WIEN2k code.[17] As for the magnetic states of $Ca_3Co_2O_6$ and $Ca_3FeRhO_6$, two ordered spin arrangements for $Ca_3Co_2O_6$ and $Ca_3FeRhO_6$ were considered: the intrachain FM state in which the spins of adjacent TP sites have a FM coupling in each $(MM'O_6)_\infty$ chain and the intrachain AFM state in which they have an AFM coupling. In both intrachain FM and AFM states the $(MM'O_6)_\infty$ chains were assumed to have a FM coupling to reduce our computational task.

**Table 1.** Relative Energies, $\Delta E = E_{AFM} - E_{FM}$ (meV/FU), of the Intrachain FM and AFM States of $Ca_3Co_2O_6$ and $Ca_3FeRhO_6$ Obtained from GGA and LDA+U Calculations with the L/APW+lo Method

| compound | GGA | LDA+U |
|---|---|---|
| $Ca_3Co_2O_6$ | 77 | −43 (with $U = 2$ eV) |
| | | 27 (with $U = 3$ eV) |
| | | 29 (with $U = 4$ eV) |
| | | −6 (with $U = 5$ eV) |
| $Ca_3FeRhO_6$ | -8 | −5 (with $U = 5.4$ eV) |

The generalized gradient approximation (GGA) of Perdew, Burke, and Ernzherof was chosen as the exchange-correlation functional.[18] For $Ca_3Co_2O_6$ the values of the atomic sphere radii were 2.6 au for Ca, 1.72 au for O, and 1.9 au for Co. For $Ca_3FeRhO_6$ the values of the sphere radii were 2.5 au for Ca, 1.80 au for O, 2.24 au for Fe, and 2.06 au for Rh. The Co 3s, Fe 3s, and Rh 4s orbitals were treated as semicore states. The plane-wave cutoff was $R_{MT} \cdot K_{max} = 7$, and up to 118 $k$ points were used for the sampling of the irreducible wedges of the Brillouin zones. The energy criterion for self-consistency was set to $10^{-4}$ Ryd per unit cell for $Ca_3Co_2O_6$ and was decreased to $10^{-5}$ Ryd for $Ca_3FeRhO_6$ because the FM and AFM solutions were close in energy. We used the experimental crystal structures of $Ca_3Co_2O_6$[19] and $Ca_3FeRhO_6$[12] determined at room temperature. In obtaining partial density of states (DOS) plots, the $z$ axis was chosen as the chain direction.

We also carried out LDA+U calculations[20,21] for $Ca_3Co_2O_6$ and $Ca_3FeRhO_6$ to see if the relative stabilities of the intrachain FM and AFM states of $Ca_3Co_2O_6$ and $Ca_3FeRhO_6$ obtained from the GGA calculations remain valid. A recent DFT study[22] of $Ca_3Co_2O_6$ with FM chains reported that DFT calculations without LDA+U are sufficient in describing its magnetic properties. Another DFT study[23] of $Ca_3Co_2O_6$ reported results of LDA+U with spin−orbit coupling calculations (hereafter referred to as the LDA+U+SOC calculations).

## 3. Spin Distributions in and Relative Energies of the Intrachain FM and AFM States

The relative energies calculated for the intrachain FM and AFM states of $Ca_3Co_2O_6$ and $Ca_3FeRhO_6$ are summarized in Table 1. According to our GGA calculations, the energy

(11) Niitaka, S.; Kageyama, H.; Kato, M.; Yoshimura, K.; Kosuge, K. *J. Solid State Chem.* **1999**, *146*, 137.
(12) Davis, M. J.; Smith, M. D.; zur Loye, H.-C. *J. Solid State Chem.* **2003**, *173*, 122.
(13) Niitaka, S.; Yoshimura, K.; Kosuge, K.; Mibu, K.; Mitamura, H.; Goto, T. *J. Magn. Magn. Mater.* **2003**, *260*, 48.
(14) For recent reviews, see: (a) Whangbo, M.-H.; Koo, H.-J.; Dai, D. *J. Solid State Chem.* **2003**, *176*, 417. (b) Whangbo, M.-H.; Dai, D.; Koo, H.-J. *Solid State Sci.* **2005**, *7*, 827.
(15) Sjöstedt, E.; Nordström, L.; Singh, D. *Solid State Commun.* **2000**, *114*, 15.
(16) Madsen, G. K. H.; Blaha, P.; Schwarz, K.; Sjöstedt, E.; Nordström, L. *Phys. Rev. B* **2001**, *64*, 195134.
(17) Blaha, P.; Schwarz, K.; Madsen, G. K. H.; Kvasnicka, D.; Luitz, J. *WIEN2k, An Augmented Plane Wave Plus Local Orbitals Program for Calculating Crystal Properties*; Vienna University of Technology: Austria, 2001.
(18) Perdew, J. P.; Burke, K.; Ernzerhof, M. *Phys. Rev. Lett.* **1996**, *77*, 3865.
(19) Fjellvåg, H.; Gulbrandsen, E.; Aasland, S.; Olsen, A.; Hauback, B. C. *J. Solid State Chem.* **1996**, *124*, 190.
(20) Anisimov, V. I.; Solovyev, I. V.; Korotin, M. A.; Czyzyk, M. T.; Sawatzky, G. A. *Phys. Rev. B* **1993**, *48*, 16929.
(21) Liechtenstein, A. I.; Anisimov, V. I.; Zaanen, J. *Phys. Rev. B* **1995**, *52*, R5467.
(22) Vidya, R.; Ravindran, P.; Fjellvåg, H.; Kjekshus, A.; Eriksson, O. *Phys. Rev. Lett.* **2003**, *91*, 186404.
(23) Wu, H.; Haverkort, M. W.; Khomskii, D. I.; Tjeng, L. H. http://arxiv.org/abs/cond-mat/0504490.

**Table 2.** Net Spin Populations of the Transition-Metal and Oxygen Atoms of $Ca_3Co_2O_6$ and $Ca_3FeRhO_6$ in the Intrachain FM and AFM States Obtained from GGA Calculations with the L/APW+lo Method

| state | compound | TP site | OCT site | O |
|---|---|---|---|---|
| FM | $Ca_3Co_2O_6$ | 2.72 | 0.33 | 0.13 |
| | $Ca_3FeRhO_6$ | 3.86 | 0.18 | 0.13 |
| AFM | $Ca_3Co_2O_6$ | 2.72 | 0.00 | 0.13 |
| | $Ca_3FeRhO_6$ | 3.89 | 0.00 | 0.15 |

difference per FU between the intrachain AFM and FM states, $\Delta E = E_{AFM} - E_{FM}$, is given by $-8$ meV/FU for $Ca_3FeRhO_6$ and 77 meV/FU for $Ca_3Co_2O_6$. These results are entirely consistent with the intrachain AFM coupling observed for $Ca_3FeRhO_6$[12−14] and the intrachain FM coupling observed for $Ca_3Co_2O_6$.[2,3,7−10] The net spin populations at the metal and oxygen atoms of $Ca_3Co_2O_6$ and $Ca_3FeRhO_6$, calculated from the integration of the up-spin and down-spin electron populations in the muffin-tin atomic spheres, are listed in Table 2. In the intrachain FM state the unpaired spin population is largely at the TP sites in both $Ca_3Co_2O_6$ and $Ca_3FeRhO_6$, while the unpaired spin population at the OCT site is smaller in $Ca_3FeRhO_6$ than in $Ca_3Co_2O_6$. To a first approximation, therefore, the OCT sites of $Ca_3Co_2O_6$ and $Ca_3FeRhO_6$ have low-spin $d^6$ cations and the TP sites high-spin $M^{3+}$ cations. This finding is consistent with the available experimental data.[3−5,13] In the intrachain AFM state the unpaired spin populations are zero at the OCT sites by symmetry in both $Ca_3Co_2O_6$ and $Ca_3FeRhO_6$.

Our LDA+U calculations for $Ca_3FeRhO_6$ with $U = 5.4$ eV show that the intrachain AFM state is more stable than the FM state by 5 meV, in good agreement with the relative stabilities of the intrachain FM and AFM states obtained from our GGA calculations. However, our LDA+U calculations for $Ca_3Co_2O_6$ reveal that the relative stabilities of the intrachain FM and AFM states depend on the $U$ value and the initial density employed for calculations. For example, the intrachain FM state is more stable than the intrachain AFM state when $U = 3$ and 4 eV (i.e., $\Delta E = 27$ and 29 meV/FU, respectively), but the opposite is true when $U = 2$ and 5 eV (i.e., $\Delta E = -43$ and $-6$ meV/FU, respectively). Thus, the ferromagnetism of $Ca_3Co_2O_6$ is reproduced by LDA+U calculations with $U \approx 3-4$ eV, which lead to $\Delta E \approx 28$ meV/FU, a value smaller than the $\Delta E$ of the GGA calculations by a factor of $\sim$0.4. The LDA+U+SOC calculations of Wu et al.,[23] using a different LDA+U scheme (i.e., Hubbard mean-field scheme), showed $\Delta E \approx 12$ meV/FU for $U = 4.1$ eV.[24] From this observation one might suggest that the $\Delta E$ value is reduced further by spin−orbit coupling.

The electronic band structure of $Ca_3Co_2O_6$ obtained from the GGA calculations shows partially filled bands, as will be presented below (section 5.1). As pointed out elsewhere,[25] it is important to recall that a system with partially filled bands can be a normal metal but is also subject to electron localization induced by electron−electron repulsion (Mott−Hubbard localization),[26] by random potential (Anderson localization) associated with lattice defects,[27] or by electron−phonon coupling as found for polaronic states.[28] Electron localization causes the extent of the electron wave function to have a finite length $L$. If this localization length $L$ is short, the electrons are strongly localized, so that the system behaves as an insulator, its charge transport occurs through hopping, and its resistivity increases strongly with decreasing the temperature. Using single-crystal samples Raquet et al.[29] found that the electrical conductivity of $Ca_3Co_2O_6$ is described by a variable range hopping mechanism with a rather high density of states at the Fermi level (i.e., $N(E_f) \approx 2.5 \times 10^{11}$ $eV^{-1}$ $m^{-1}$). Therefore, the electronic band structure of $Ca_3Co_2O_6$ obtained from the GGA calculations, which show partially filled bands, is consistent with the experimental result of Raquet et al. In the study of Wu et al.[23] the hopping conductivity of $Ca_3Co_2O_6$ was explained by introducing a band gap at the Fermi level on the basis of LDA+U+SOC calculations. However, this explanation makes $N(E_f) = 0$, which is inconsistent with the experimental finding that $N(E_f) \neq 0$. In view of this observation, the validity of LDA+U or LDA+U+SOC calculations for $Ca_3Co_2O_6$ is doubtful. As pointed out by Johannes et al. in their study of $Na_xCoO_2$,[30] use of LDA+U calculations requires caution and may lead to a worse agreement with experimental data than do simple LDA calculations. In addition, it should be recalled that $U$ is an empirical parameter in LDA+U or LDA+U+SOC calculations. Therefore, in the following we will focus our discussion on our GGA calculations.

### 4. Effective Orbital Energies in Spin-Polarized Electronic Structure

The plots of the total and partial density of states (DOS) calculated for the nonmagnetic states of $Ca_3Co_2O_6$ and $Ca_3FeRhO_6$ are presented in Figure 2. The nature of the d-block bands and the occurrence of a band gap at the Fermi level in the nonmagnetic state are readily explained in terms of the d-block levels of an isolated $CoO_6$ octahedron and an isolated $CoO_6$ trigonal prism depicted in Figure 3, which were obtained from extended Hückel tight binding calculations.[31] The bottom three levels of the $CoO_6$ trigonal prism lie below those of the $CoO_6$ octahedron and are each doubly occupied in the low-spin $Co^{3+}$ configuration. For a low-spin $Fe^{3+}$ ion at the TP site, one of the bottom three levels becomes half-filled. The d-block bands of the nonmagnetic states (Figure 2) show a band gap for $Ca_3Co_2O_6$ and a partially filled band for $Ca_3FeRhO_6$, which are a consequence

(24) Wu et al. used the value of $U = 5$ eV, which corresponds to $U - J_H = 5 - 0.9 = 4.1$ eV in our LDA+U scheme.

(25) Gourdon, O.; Evain, M.; Jobic, S.; Brec, R.; Koo, H.-J.; Whangbo, M.-H. *Inorg. Chem.* **2001**, *40*, 2898.

(26) Mott, N. F. *Metal−Insulator Transitions*, 2nd ed.; Taylor & Francis: New York, 1990.

(27) Hayes, W.; Stoneham, A. M. *Defects and Defect Processes in Nonmetallic Solids*; Wiley: New York, 1985.

(28) Schlenker, C.; Marezio, M. *Philos. Mag. B* **1980**, *42*, 453.

(29) Raquet, B.; Baibich, M. N.; Broto, J. M.; Rakoto, H.; Lambert, S.; Maignan, A. *Phys. Rev. B* **2002**, *65*, 104442.

(30) Johannes, M. D.; Mazin, I. I.; Singh, D. J. *Phys. Rev. B* **2005**, *71*, 205103.

(31) Our calculations were carried out by employing the SAMOA (Structure and Molecular Orbital Analyzer) program package (Dai, D.; Ren, J.; Liang, W.; Whangbo, M.-H. http://chvamw.chem.ncsu.edu/, 2002).

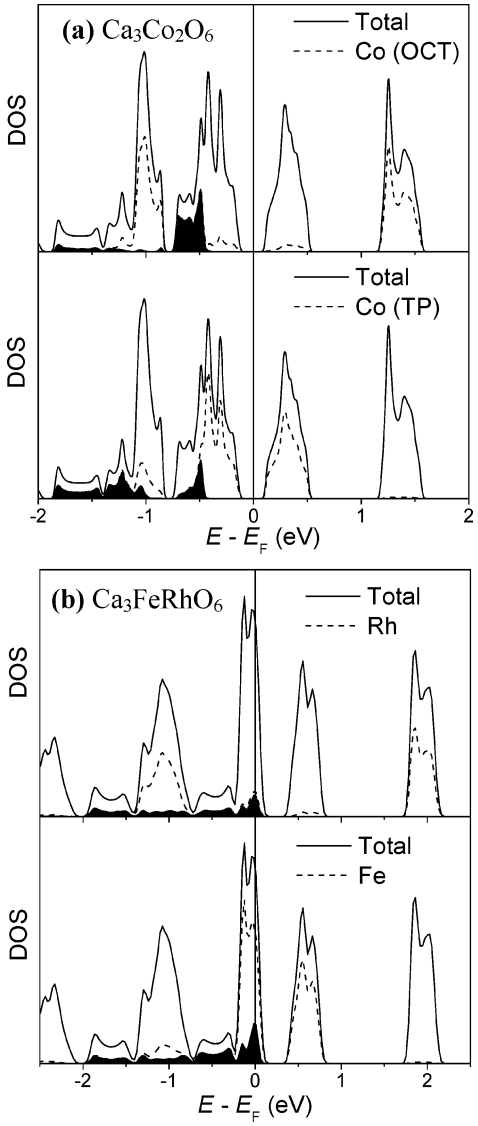


**Figure 2.** Total and partial DOS plots for the nonmagnetic state of (a) $Ca_3Co_2O_6$ and (b) $Ca_3FeRhO_6$ obtained from GGA calculations with the L/APW+lo method. The partial DOS plots for the $d_{z^2}$ orbitals of the transition-metal atoms are indicated by shading.

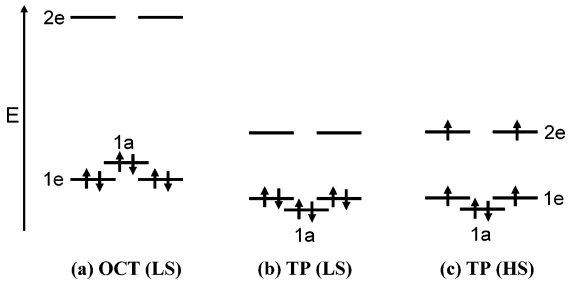


**Figure 3.** Occupations of the effective one-electron d-block levels for (a) the low-spin $Co^{3+}$ ion at an OCT site, (b) the low-spin $Co^{3+}$ ion at a TP site, and (c) the high-spin $Co^{3+}$ ion at a TP site of $Ca_3Co_2O_6$.

of the low-spin electron configurations at the OCT and TP sites. With the 3-fold rotational axis of a $(Co_2O_6)_\infty$ chain taken as the $z$ axis, the $d_{z^2}$ orbital of a $CoO_6$ octahedron becomes one of its $t_{2g}$ orbitals[32] and that of a $CoO_6$ trigonal prism becomes the lowest-lying d-block level of the trigonal prism (i.e., the 1a levels of Figure 3).

In DFT magnetic states are described by spin-polarized electronic structures, which give rise to different orbital compositions and different energy levels for up-spin and down-spin bands, in contrast to the case of nonmagnetic states. Thus, in describing the results of spin-polarized electronic structure calculations for $Ca_3Co_2O_6$ and $Ca_3FeRhO_6$ in the next section, it is crucial to know how the effective d-block levels of the TP- and OCT-site metal ions depend on the number of unpaired spins and the associated electron−electron repulsion. For simplicity, we restrict our discussion to the up-spin and down-spin $d_{z^2}$ levels at the TP and OCT sites of $Ca_3Co_2O_6$ and denote the $d_{z^2}$ levels of the OCT and TP sites in the absence of electron−electron repulsion as $e_o$ and $e_t$, respectively. In the presence of electron−electron repulsion, the up-spin and down-spin $d_{z^2}$ levels of the low-spin OCT and the high-spin TP sites of $Ca_3Co_2O_6$ are expressed as[33−36]

$$e_o\uparrow = e_o\downarrow \approx e_o + U + 4U' - 2K$$

$$e_t\uparrow \approx e_t + U + 4U' - 4K$$

$$e_t\downarrow \approx e_t + U + 4U' \quad (1)$$

where $U$ is the on-site Coulomb repulsion for two electrons in a same metal d orbital, $U'$ is that for two electrons in two different metal d orbitals, and $K$ is the exchange repulsion between two electrons of an identical spin in two different d orbitals. Then the energy differences between the up-spin and down-spin $d_{z^2}$ levels are given by

$$(e_o\uparrow - e_t\uparrow) \approx e_o - e_t + 2K$$

$$(e_o\downarrow - e_t\downarrow) \approx e_o - e_t - 2K \quad (2)$$

The energy levels of the $CoO_6$ octahedron and trigonal prism presented in Figure 3 show that $e_o - e_t > 0$ for $Ca_3Co_2O_6$ (i.e., $e_o - e_t = 0.14$ eV). Thus, due to the exchange integral $K$, the up-spin $d_{z^2}$ levels have a greater energy difference than does the down-spin $d_{z^2}$ levels, i.e., $(e_o\uparrow - e_t\uparrow) > (e_o\downarrow - e_t\downarrow)$. Consequently, the adjacent TP and OCT sites should have a stronger orbital interaction (i.e., a stronger covalent interaction) for the down-spin $d_{z^2}$ levels than for the up-spin $d_{z^2}$ levels.[37]

## 5. Spin-State-Dependent Metal−Metal Bonding

**5.1. Ferromagnetic Coupling.** The total and partial DOS plots obtained from GGA calculations for the FM state of $Ca_3Co_2O_6$ are shown in Figure 4. The relative ordering of these four subbands is in agreement with that of the $d_{z^2}$ orbitals shown in eq 1. The down-spin $d_{z^2}$ bands have both

(32) Whangbo, M.-H.; Koo, H.-J.; Dai, D.; Villesuzanne, A. *J. Solid State Chem.* **2002**, *165*, 345.

(33) Brandow, B. H. *Adv. Phys.* **1977**, *26*, 651.
(34) Whangbo, M.-H. *Inorg. Chem.* **1980**, *19*, 1728.
(35) Pouchard, M.; Villesuzanne, A.; Doumerc, J.-P. *J. Solid State Chem.* **2001**, *162*, 282.
(36) Whangbo, M.-H.; Koo, H.-J.; Villesuzanne, A.; Pouchard, M. *Inorg. Chem.* **2002**, *41*, 1920.
(37) Albright, T. A.; Burdett, J. K.; Whangbo, M.-H. *Orbital Interactions in Chemistry*; Wiley: New York, 1985; Chapter 2.

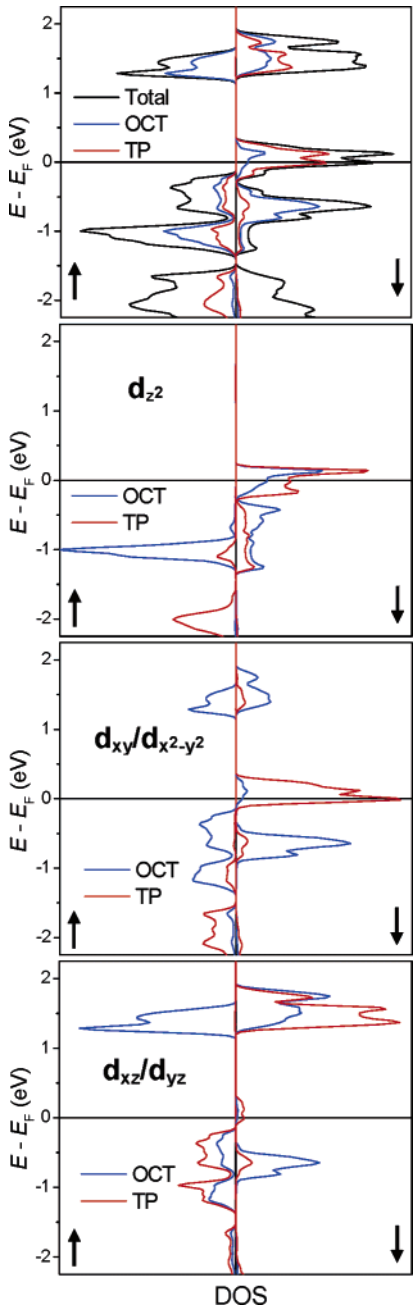


**Figure 4.** Total and partial DOS plots for the intrachain FM state of $Ca_3Co_2O_6$ obtained from GGA calculations with the L/APW+lo method.

OCT and TP character and show a shape characteristic of 1D bands expected from overlap between the $d_{z^2}$ orbitals of adjacent OCT and TP sites. In other words, the extent of the orbital mixing between the $d_{z^2}$ levels of the OCT and TP sites is much stronger in the down-spin $d_{z^2}$ bands than in the up-spin $d_{z^2}$ bands. This is readily explained on the basis of eq 2 assuming that $e_t - e_o \approx 2K$. Under this assumption the $e_o\uparrow$ and $e_t\uparrow$ levels are nearly degenerate (i.e., $e_o\uparrow \approx e_t\uparrow$) and the $e_t\downarrow$ and $e_o\downarrow$ levels are nondegenerate (i.e., $e_t\downarrow \approx e_o\downarrow + 4K$). Therefore, the 1D band formation and the strong metal−metal interaction in the down-spin $d_{z^2}$ states of $Ca_3Co_2O_6$ arise from an accidental degeneracy of the $e_o\downarrow$ and $e_t\downarrow$ levels. In addition, the Co···Co distance through the shared triangular face is short (i.e., 2.595 Å),[19] so that the $d_{z^2}$ orbitals of adjacent TP and OCT sites can overlap significantly, thus leading to the wide down-spin $d_{z^2}$ bands.

The up-spin $d_{xy}/d_{x^2-y^2}$ bands of largely TP character are completely filled, and so are the up-spin $d_{xz}/d_{yz}$ bands of largely TP character, as expected from the high-spin electron configuration of a TP-site $Co^{3+}$ ion in Figure 3. Of the two subbands of the down-spin $d_{z^2}$ bands, the upper subband with slightly stronger TP character is partially empty while the down-spin $d_{xy}/d_{x^2-y^2}$ bands of largely TP character are partially filled (Figure 4). The upper subband of the down-spin $d_{z^2}$ bands has an orbital character of metal−metal $\sigma$ antibonding, while the down-spin $d_{xy}/d_{x^2-y^2}$ bands have no metal−metal interaction. Thus, the "electron transfer" from the upper subband of the down-spin $d_{z^2}$ bands to the down-spin $d_{xy}/d_{x^2-y^2}$ bands strengthens metal−metal bonding between adjacent cobalt atoms in each $(Co_2O_6)_\infty$ chain and also induces a small unpaired spin population at the OCT site (0.33 electrons).

The total and partial DOS plots obtained from GGA calculations for the intrachain FM state of $Ca_3FeRhO_6$ are presented in Figure 5. The electronic structure of $Ca_3FeRhO_6$ exhibits features similar to those found for $Ca_3Co_2O_6$. However, there are important differences. In contrast to $Ca_3Co_2O_6$, the lower and upper subbands of the down-spin $d_{z^2}$ bands are separated by a band gap (0.33 eV) in $Ca_3FeRhO_6$. Furthermore, $Ca_3FeRhO_6$ shows a much stronger TP character in the upper subband of the down-spin $d_{z^2}$ bands and a much stronger OCT character in the lower subband of the down-spin $d_{z^2}$ bands. This indicates that in $Ca_3FeRhO_6$ the down-spin $d_{z^2}$ level $e_o\downarrow$ of the OCT site is considerably lower in energy than the down-spin $d_{z^2}$ level $e_t\downarrow$ of the TP site. In the nonmagnetic state of $Ca_3FeRhO_6$ the $d_{z^2}$ bands of the TP (Fe) and OCT (Rh) sites are similar in energy (Figure 2b) and thus form a wide 1D band. Under spin polarization, this degeneracy is lifted and the OCT $d_{z^2}$ bands lie between the up- and down-spin TP $d_{z^2}$ bands (Figure 5). Therefore, the direct metal−metal interaction in the intrachain FM state becomes much less efficient in $Ca_3FeRhO_6$ than in $Ca_3Co_2O_6$.

Since $Ca_3FeRhO_6$ has one less valence electron per FU than does $Ca_3Co_2O_6$, the upper subband of the down-spin $d_{z^2}$ bands is empty in $Ca_3FeRhO_6$. In $Ca_3FeRhO_6$ the down-spin $d_{xy}/d_{x^2-y^2}$ bands of TP character are not filled and the spin density at the OCT site is reduced by a factor of almost two when compared with the case of $Ca_3Co_2O_6$ (Table 2).

**5.2. Antiferromagnetic Coupling.** The total and partial DOS plots calculated for the intrachain AFM state of $Ca_3Co_2O_6$ are shown in Figure 6. In contrast to the intrachain FM state, the up-spin and down-spin $d_{z^2}$ bands of the intrachain AFM state are very narrow. In the intrachain AFM state the TP sites are divided into the up-spin and down-spin sites. In the up-spin $d_{z^2}$ bands the $d_{z^2}$ orbitals of only the up-spin TP sites interact with those of their adjacent OCT sites. Likewise, in the down-spin $d_{z^2}$ bands the $d_{z^2}$ orbitals of only the down-spin TP sites interact with those of the adjacent OCT sites. Thus, in either the up-spin or down-spin band the direct metal−metal bonding can take place only within each "OCT−TP−OCT" cluster unit of every $(Co_2O_6)_\infty$ chain. Effectively, therefore, the extent of direct

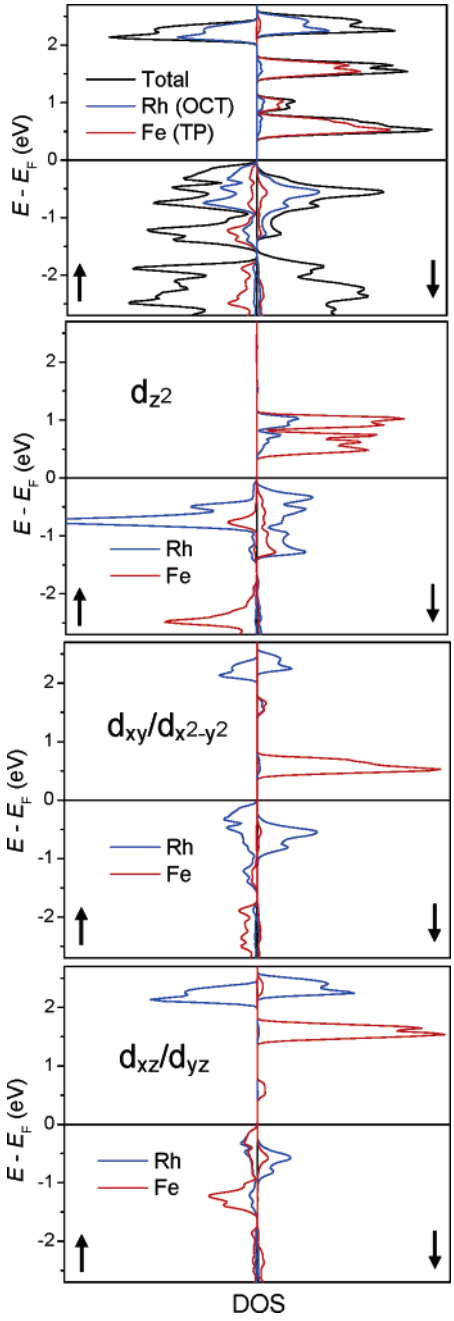


**Figure 5.** Total and partial DOS plots calculated for the intrachain FM state of $Ca_3FeRhO_6$ obtained from GGA calculations with the L/APW+lo method.

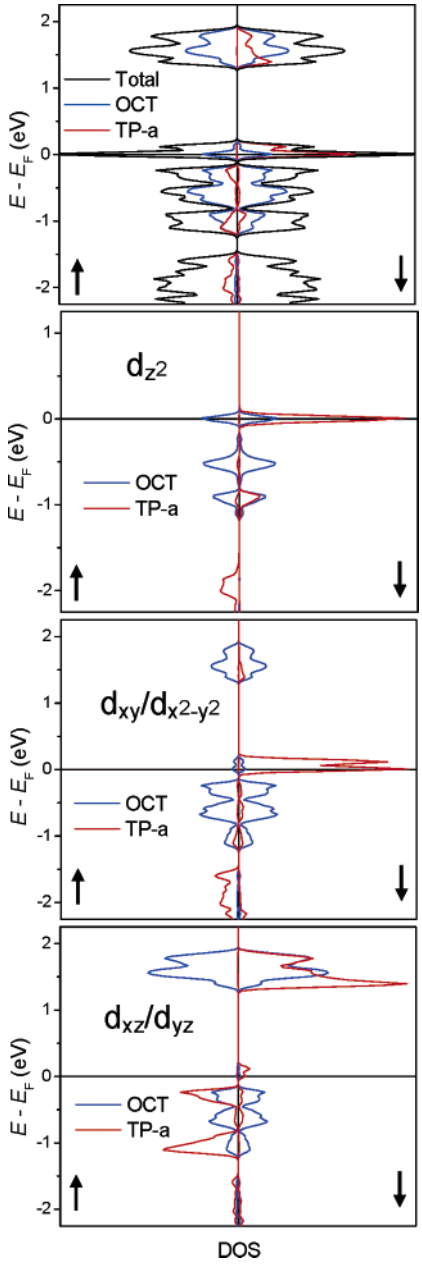


**Figure 6.** Total and partial DOS plots for the intrachain AFM state of $Ca_3Co_2O_6$ obtained from GGA calculations with the L/APW+lo method.

metal−metal interaction between adjacent cobalt atoms is reduced in the intrachain AFM state, so that its $d_{z^2}$ bands are narrow. Similar observations are found from the total and partial DOS plots calculated for the AFM state of $Ca_3FeRhO_6$ shown in Figure 7. Nevertheless, in the intrachain FM state of $Ca_3FeRhO_6$ (Figure 5) the down-spin $d_{z^2}$ bands of OCT and TP character are already well separated in energy, i.e., the direct metal−metal bonding interaction is weak. Thus, on going from the intrachain FM to the intrachain AFM state, the energy loss associated with losing direct metal−metal bonding is much weaker in $Ca_3FeRhO_6$ than in $Ca_3Co_2O_6$.

In the intrachain AFM state of $Ca_3Co_2O_6$ the $d_{z^2}$ bands of largely TP character are partially empty while the $d_{xy}/d_{x^2-y^2}$ bands of largely TP character are partially occupied. As discussed in the previous section, this feature is also present in the intrachain FM state of $Ca_3Co_2O_6$. This indicates that the down-spin $d_{z^2}$ orbital of the TP site is close in energy to the down-spin $d_{xy}/d_{x^2-y^2}$ orbital of the TP site.

## 6. Concluding Remarks

The intrachain ferromagnetism in $Ca_3Co_2O_6$ is explained in terms of the spin-state-dependent metal−metal interactions. The intrachain FM coupling is strongly favored over the intrachain AFM coupling in $Ca_3Co_2O_6$ because a stronger direct metal−metal bonding is allowed to take place between adjacent cobalt atoms in each $(Co_2O_6)_\infty$ chain in the intrachain

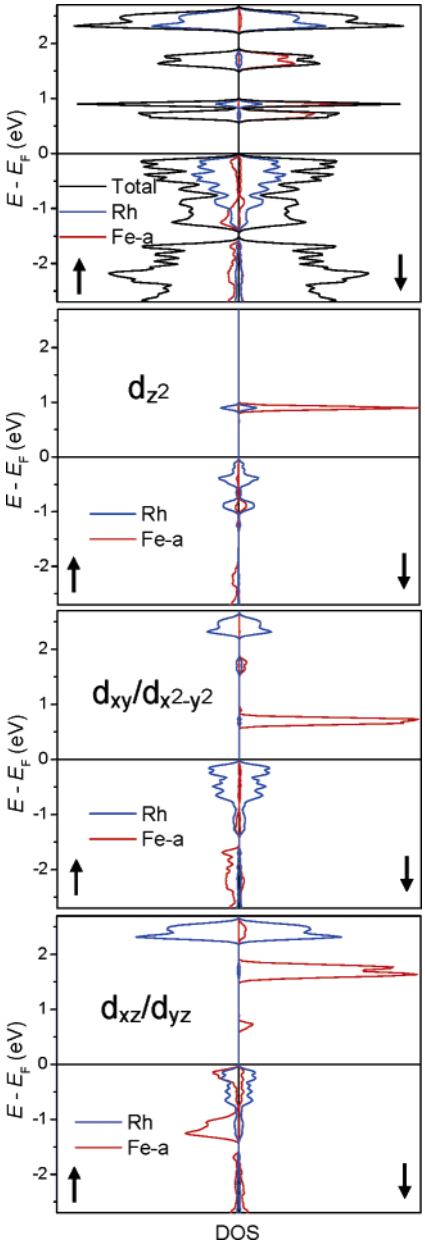


**Figure 7.** Total and partial DOS plots calculated for the intrachain AFM state of $Ca_3FeRhO_6$ obtained from GGA calculations with the L/APW+lo method.

FM state than in the intrachain AFM state. The down-spin $d_{z^2}$ orbital levels of the OCT- and TP-site $Co^{3+}$ ions are similar in energy (accidental degeneracy) and orbital extension, and the nearest-neighbor Co−Co distance in each $(Co_2O_6)_\infty$ chain of $Ca_3Co_2O_6$ is short (i.e., 2.595 Å). Consequently, in the intrachain FM state the extent of direct metal−metal bonding between adjacent TP and OCT sites should be significant in $Ca_3Co_2O_6$. Ferromagnetism in materials arises from several different mechanisms, which include Stoner,[38] double exchange,[39] spin exchange,[40] and spin polarization[41] mechanisms. The intrachain ferromagnetism of $Ca_3Co_2O_6$, which is not explained by any of these mechanisms, might be referred to as a metal−metal-bonding-induced ferromagnetism. This mechanism should be applicable to magnetic insulators and magnetic metals of transition-metal elements in which direct metal−metal bonding can be enhanced by ferromagnetic ordering. For example, $Ca_3CoRhO_6$[42] is isoelectronic and isostructural with $Ca_3Co_2O_6$ and shows an intrachain ferromagnetism as does $Ca_3Co_2O_6$. In the rare-earth intermetallic compound $PrMnSi_2$,[43] which consists of isolated layers of Mn atoms, the Mn atoms of each Mn layer are ferromagnetically coupled with ferromagnetic ordering between the Mn layers up to $T_C = 434$ K.

In $Ca_3FeRhO_6$ the down-spin $d_{z^2}$ orbitals of the high-spin $Fe^{3+}$ and low-spin $Rh^{3+}$ ions differ in energy and orbital extension, and the nearest-neighbor Fe−Rh distance in each $(FeRhO_6)_\infty$ chain of $Ca_3FeRhO_6$ is longer than the nearest-neighbor Co−Co distance in each $(Co_2O_6)_\infty$ chain of $Ca_3Co_2O_6$ (i.e., 2.694 vs 2.595 Å). Consequently, in the intrachain FM state the extent of the direct metal−metal bonding between adjacent TP and OCT sites should be weaker in $Ca_3FeRhO_6$ than in $Ca_3Co_2O_6$. As a result, the spin moments of $Ca_3FeRhO_6$ are largely localized on the TP sites, and hence, the spin exchange between adjacent TP sites becomes dominated by AFM interactions through the Fe−O···O−Fe super-superexchange paths.

**Acknowledgment.** The work at NCSU was supported by the Office of Basic Energy Sciences, Division of Materials Sciences, U.S. Department of Energy, under Grant DE-FG02-86ER45259. The authors thank the Pole M3PEC, Bordeaux 1 University, France, for computing resources.

IC0508775

(38) Stoner, E. C. *Proc. R. Soc. A* **1938**, *165*, 372.
(39) Zener, C. *Phys. Rev.* **1951**, *82*, 403.
(40) Goodenough, J. B. *Magnetism and the Chemical Bond*, Wiley: Cambridge, MA, 1963.
(41) Kahn, O. *Molecular Magnetism*, VCH: New York, 1993; Chapter 12.
(42) Niitaka, S.; Yoshimura, K.; Kosuge, K.; Nishi, M.; Kakurai, K. *Phys. Rev. Lett.* **2001**, *87*, 177202−1 and references therein.
(43) Szytula, A.; Leciejewicz, J. *Handbook of crystal structures and magnetic properties of rare earth intermetallics;* CRC Press: Ann Arbor, MI, 1994.